

CVD of pure copper films from novel iso-ureate complexes†

Cite this: *Dalton Trans.*, 2013, **42**, 5554

Alexander M. Willcocks,^a Thomas Pugh,^a Jeff A. Hamilton,^a Andrew L. Johnson,^{*a} Stephen P. Richards^b and Andrew J. Kingsley^b

We report the synthesis and characterisation of a new family of copper(i) metal precursors based around alkoxy-*N,N'*-di-alkyl-ureate ligands, and their subsequent application in the production of pure copper thin films. The molecular structure of the complexes bis-copper(i)(methoxy-*N,N'*-di-isopropylureate) (**1**) and bis-copper(i)(methoxy-*N,N'*-di-cyclohexylureate) (**5**) are described, as determined by single crystal X-ray diffraction analysis. Thermogravimetric analysis of the complexes highlighted complex **1** as a possible copper CVD precursor. Low pressure chemical vapour deposition (LP-CVD) was employed using precursor **1**, to synthesise thin films of metallic copper on ruthenium substrates under an atmosphere of hydrogen (H₂). Analysis of the thin films deposited at substrate temperatures of 225 °C, 250 °C and 300 °C, respectively, by SEM and AFM reveal the films to be continuous and pin hole free, and show the presence of temperature dependent growth features on the surface of the thin films. Energy dispersive X-ray spectroscopy (EDX), powder X-ray diffraction (PXRD) and X-ray photoelectron spectroscopy (XPS) all show the films to be high purity metallic copper.

Received 11th January 2013,

Accepted 5th February 2013

DOI: 10.1039/c3dt00104k

www.rsc.org/dalton

Introduction

The production of metallic thin films by chemical vapour deposition (CVD),¹ or more recently atomic layer deposition (ALD)² has been an area of significant interest to those in the microelectronics industry for the last three decades, mainly due to numerous potential applications in which these materials can be exploited.^{1*d,e*,2*a,b*} During this time the deposition of copper has continually been at the forefront of research, and the 2011 International Technology Roadmap for Semiconductors (ITRS) predicts that copper will remain the primary interconnect material throughout the next 15 years, although there are some technical challenges still to overcome. As the size-downscaling of microelectronics continues, the use of copper as an interconnect material in integrated circuitry and the chip fabrication process has increased.^{1*c,e*,2*b*} The physical properties that make copper so desirable for such applications include its very low resistivity (significantly lower than aluminium and much lower than tungsten) and

electromigration resistance that is far superior to that of aluminium (though inferior to tungsten). Industrially, copper interconnects/seed layers are deposited onto a ruthenium 'glue layer' which allows for better adhesion to common barrier layers such as TiN and TaN, which are necessary to inhibit diffusion of copper into the underlying substrates, such as Si and SiO₂, in microelectronic devices.³

Over the past few years a great deal of effort has been employed on research into ternary and quaternary compound semiconductors; namely copper indium diselenide (CIS), copper indium gallium diselenide (CIGS) and copper zinc tin sulfide (CZTS) have shown excellent solar cell properties.⁴ Thin film CIGS based solar cells have been produced with an efficiency of up to 20%.⁵ One of the techniques used to form CIGS layers is a two-stage approach which involves the deposition of a precursor layer (*e.g.* Cu) on a substrate followed by a high temperature activation step (reaction with Se or S) that converts the precursor layer into solar cell grade semiconductor materials.⁶

As a result of this interest, considerable research into the development of copper metal precursors for CVD and ALD application has been described, and examples of potential precursors^{1*d*} include Cu(i) organometallics,⁷ Cu(i) and Cu(ii) β -diketonate,⁸ β -ketoiminate^{2*i,9*} and β -ketoesterate¹⁰ complexes as well as Cu(i) and Cu(ii) carboxylates,¹¹ and alkoxide complexes.¹² Typically precursors based around Cu(i) are quite volatile and have low deposition temperatures, whereas Cu(ii) systems are on average rather too stable, and show low

^aDepartment of Chemistry, University of Bath, Bath, BA13 3DN, UK.

E-mail: A.L.Johnson@bath.ac.uk

^bSAFC-Hitech, Power Road, Bromborough, Wirral, CH62 3QF, UK

†Electronic supplementary information (ESI) available: Supporting information includes the EXD spectra for Cu films grown at 250 °C and 300 °C as well as XPS spectra for the same films (pre- and post-A-etching). A powder X-ray diffraction spectra of the Ru substrate used throughout this study is also included. CCDC 901461–901465. For ESI and crystallographic data in CIF or other electronic format see DOI: 10.1039/c3dt00104k

volatility, need high deposition temperatures and require reducing carrier gases *e.g.* H₂ to activate them. It is therefore the desire to combine the best of these features that has directed new attention towards the development of Cu(I) based precursors.

Recently, copper(I) amidinate^{2c,e,f,h,j,13} and guanidinate^{13,14} complexes have received attention as potential precursors for the deposition of pure copper thin films, because of their relative air stability, thermal stability and lack of oxygen within the ligands system. Closely related to formamidinate, amidinate, guanidinate and triazenide ligands, are *O,N,N'*-trisubstituted iso-ureate ligand (alternatively named pseudoureas),¹⁵ which differ only by virtue that they contain an alkoxide, {OR}, substituent at the central carbon atom of the {NCN} moiety rather than an H-atom (formamidinate), alkyl/aryl group (amidinate) or an amine group *i.e.* {NR₂} or {NHR} (guanidinate). Together with the triazenide ligands, these systems are iso-electronic and as such should share common structural and electronic features (Fig. 1), an observation which is apparent in the case of copper amidinate and copper guanidinate complexes.

For guanidinate and iso-ureate ligands the possibility exists of significant lone-pair interaction and delocalisation of electron density from the {NR₂} or {OR} substituents into the {NCN} core. Any such delocalisation has a substantive effect on the orientation of either the {NR₂} or {OR} moiety, as shown in Fig. 1. In the case of the iso-ureate ligands the oxygen atom of the {OR} group can be either considered as sp³, sp² or sp hybridised: for an sp³ hybridisation there is no exocyclic π-bonding as both lone pairs of electrons are orientated away from the delocalized {NCN} unit. For a sp² hybridised oxygen atom the C–O–R angle of the iso-ureate should ideally approach 120°. For delocalisation of electron density to occur the p-orbital based lone pair needs to be coplanar with

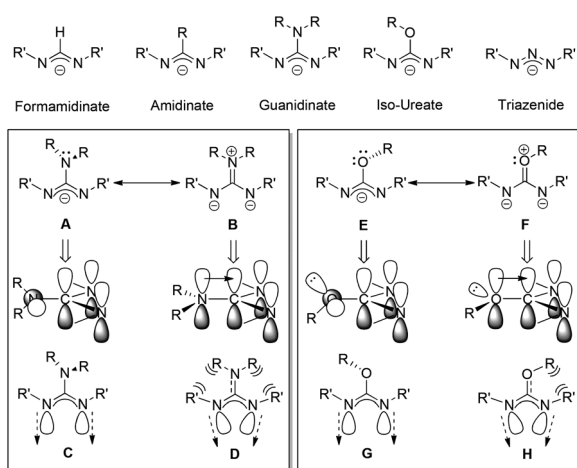


Fig. 1 General structure of formamidinate, amidinate, guanidinate, iso-ureate and triazenide anions. Comparative resonance forms of the guanidinate and iso-ureate; showing the effect of orientation, and lone pair interaction (A, B, E and F) with the π-delocalised {NCN} core, on the steric interactions and N-orbital projections (C, D, G and H) within the ligand.

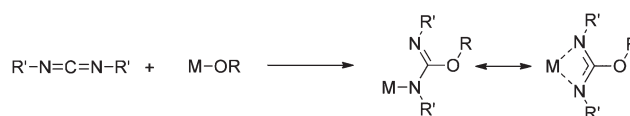
the delocalised {NCN} unit. Similarly, with an sp hybridised oxygen centre, π-bonding to the {NCN} unit imposes a planarity with one of the two p-orbital based lone pairs, but more importantly the C–O–R angle will tend towards linearity (180°). Any degree of π-bonding to the {NCN} unit will be accompanied by a reduction in C–O bond length as the multiple bond character of this exocyclic bonding increases, as well as a change in the pyramidalisation of the amide nitrogen atoms; caused, in part, by steric interactions between the oxygen substituents and the substituents on the {NCN} core. Similar arguments have been presented for metal guanidinate complexes elsewhere.^{14c}

Despite the fact that the addition of alcohols into carbodiimides to form *O,N,N'*-trisubstituted iso-ureas (R'NC(OR)NHR') have been known since the early 1900's there is a paucity of data concerning the formation of metal iso-ureate complexes. In an analogous manner to amidinate and guanidinate complexes formed by the insertion of carbodiimides into M–C and M–N bonds respectively, there are reports that describe the formation of iso-ureate complexes by the insertion of carbodiimides into Mg–OMe,¹⁶ Ti–OⁱPr,¹⁷ Sn–OMe¹⁸ and Pb–OMe¹⁹ bonds (Scheme 1), although characterising data for these products is limited.¹⁶

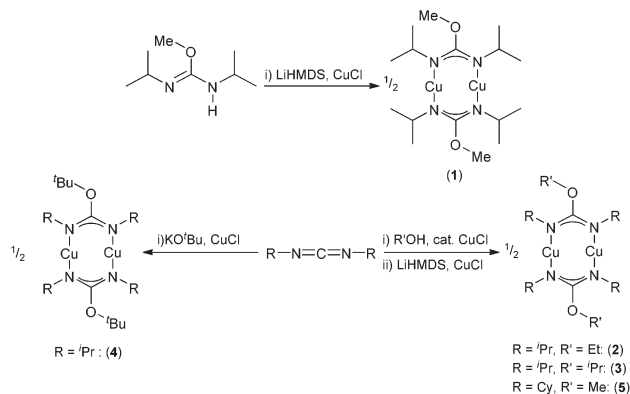
There are also several comprehensively characterised examples of adducts formed between carbodiimides and metal alkoxide complexes, hinting at a reduced reactivity of the alkoxides towards insertion compared to metal amide complexes.²⁰

While several coordination complexes and adducts of iso-ureas are known, examples are limited.²¹ Similarly, reactions between *O,N,N'*-trisubstituted iso-ureas with metal alkyl or amide complexes are also limited, and restricted to examples involving cyclic-iso-ureas (alternatively named amino-oxazolines).²² However, copper iso-ureate complexes have appeared in the patent literature.²³

The dearth of fully characterised iso-ureate complexes, coupled with the range of derivatives that are potentially available through substitution at the terminal nitrogen atoms and the {OR} group, which allow the tunability of important features such as volatility, stability and reactivity, makes such complexes an appealing area of study. We report here the synthesis and characterisation of a new family of copper metal precursors based around the novel iso-ureate ligands and the subsequent utility of these new precursors in the production of pure, continuous, copper thin films deposited onto ruthenium substrates at a range of substrate temperatures by low pressure chemical vapour deposition (LP-CVD).



Scheme 1 The general insertion of metal alkoxides into carbodiimides.



Scheme 2 Synthesis of the copper(I) iso-ureate complexes 1–5.

Results and discussion

Synthesis and molecular structures

Of the iso-ureas used in this study (Scheme 2) only the methoxy-*N,N'*-di-isopropylurea, is commercially available. The potassium salt of *t*-butoxy *N,N'*-di-isopropylurea can be efficiently formed *in situ* by the reaction of potassium *tert*-butoxide with *N,N'*-diisopropylcarbodiimide. The remaining urea ligands were synthesised by the CuCl catalysed (~0.075 mol% CuCl per mmol of carbodiimide) reaction of carbodiimide with equimolar amounts, or greater, of primary, secondary, or tertiary alcohols without solvents at room temperature in a slightly exothermic reaction. Subsequent filtration of the reaction mixture and addition to a THF solution of Lithium hexamethyldisilylamide (LiHMDS) affords the desired lithium iso-ureate *in situ*.

All Cu(I) iso-ureate compounds shown in Scheme 2, were synthesised by reaction of anhydrous CuCl with the corresponding lithium iso-ureate in THF at ambient temperature to afford the final products. All of the products were soluble in hexane, and extraction followed by recrystallisations at $-28\text{ }^{\circ}\text{C}$ afforded pure products as colourless or pale yellow crystalline solids (yield 58–74%). In all case products were characterised by ^1H , $^{13}\text{C}\{^1\text{H}\}$ NMR spectroscopy, elemental analysis and single crystal X-ray diffraction.

The ^1H NMR spectra of the complexes 1–4, all contain a doublet between $\delta = 1.11\text{--}1.14$ ppm and a septet between $\delta = 3.67\text{--}3.80$ ppm, which correspond to the methyl and methine protons of the isopropyl groups, respectively. Additional signals were observed for the {OMe}, {OEt}, {O^{*i*}Pr} and {O^{*t*}Bu} groups in the expected coupling patterns and intensity ratios. Similarly, the ^{13}C NMR spectra of the complexes show resonances between $\delta = 27.2\text{--}28.0$ ppm for the methyl carbons, and between $\delta = 46.5\text{--}47.8$ ppm for the methine carbons. The spectra for 1–4 also contain a common resonance between $\delta = 165.31\text{--}167.692$ ppm, which is attributed to the central carbon atom of the {NCN} moiety. Resonances are also observed for the {OMe} ($\delta = 59.6$ ppm), {OEt} ($\delta = 15.2, 67.9$ ppm), {O^{*i*}Pr} ($\delta = 22.3, 73.8$ ppm) and {O^{*t*}Bu} ($\delta = 30.0, 80.5$ ppm) moieties in the $^{13}\text{C}\{^1\text{H}\}$ NMR spectra.

The ^1H NMR spectrum of complex 5 consists of four multiplets for the cyclohexyl protons ($\delta = 1.21, 1.50, 1.64, 1.93$ ppm) and a singlet for the {OMe} protons ($\delta = 3.39$ ppm). Correspondingly the ^{13}C NMR spectrum contains the six resonances attributed to the cyclohexyl group, the methoxy group and the central NCN carbon at $\delta = 26.7, 27.0, 39.7, 55.9, 60.0$ and 168.2 ppm respectively. In all cases the solution state NMR studies are consistent with the formation of dimeric complexes of the general formula $[\text{Cu}_2(\text{L})_2]$ (L = iso-urea).

Single crystal X-ray quality crystals of all the complexes described in this paper were grown from hexane solution at $-28\text{ }^{\circ}\text{C}$. All the iso-ureate complexes described in this study are dimeric and show common gross structural features. The molecular structures of the complexes 1 and 5, discussed below, are shown in Fig. 2 and are taken as demonstrators of common structural features in both the isopropyl and cyclohexyl substituted iso-ureates. Selected bond lengths and angles are shown in Fig. 2. Complexes 2–4 are isostructural to complex 1, with the only significant differences in the molecular structures focused on the relative orientation of the {OR} moiety. The molecular structures of complexes 2–4 along with bond lengths and bond angles are provided in the ESI† for this paper. Crystal data and collection parameters for complexes 1–5 are shown in Experimental section of this paper (Table 4).

For both 1 and 5, the copper metal atoms are bridged by two iso-ureate ligands in a μ, η^1, η^1 -fashion. Unlike structurally related copper(I) guanidinate complexes, which in the solid state show significant twisting of the $\{\text{Cu}_2(\text{N}_2\text{C})_2\}$ core at the Cu–Cu axis,^{14a,c} the iso-ureate complexes 1–5 show no such disruption. Both $\{\text{Cu}_2(\text{N}_2\text{C})_2\}$ cores are planar [RMS deviation of the fitted atoms: 0.0119 \AA (for 1) and 0.0068 \AA (for 5)]. It is also noteworthy that unlike the comparable guanidinate complexes, where a change in the N-substituent from iso-propyl to cyclohexyl results in a significant twisting of the core. No such observation is made for the iso-ureate complexes 1 and 5, as can be seen from the least-squares overlay of the two complexes (Fig. 3).

In both complexes the geometries about the two-coordinate metal atoms approach linearity [for 1: $\text{N}(1)\text{--Cu}(1)\text{--N}(3) = 176.04(9)^\circ$ and $\text{N}(2)\text{--Cu}(1)\text{--N}(4) = 175.11(9)^\circ$; for 5: $\text{N}(1)\text{--Cu}(1)\text{--N}(2\text{A}) = 175.83(10)^\circ$], with the deviation presumably the result of inter-nuclear Cu...Cu repulsion. In both complexes, the metal–metal distances [Cu(1)–Cu(2): $2.4653(4)\text{ \AA}$ and Cu(1)–Cu(1A): $2.4624(7)\text{ \AA}$ respectively], which are comparable to related di-copper amidinate, guanidinate, and triazenide complexes, are significantly shorter than the sum of the Van der Waals radii of Cu (1.40 \AA), suggesting the possible presence of $d^{10}\text{--}d^{10}$ metallophilic interaction, although this is a matter of some debate in the literature.²⁴ The Cu–N bond distances in 1–5 are within the expected ranges for terminal Cu(I)–N bonds.^{2c,f,13,14c,23,24} Similarly the N–C bond lengths within the iso-ureate ligands are also comparable to those observed in related systems.

As noted earlier, the relative orientation of the {OR} substituent can give some indication, along with $\{\text{N}_2\text{C}\text{--OR}\}$ bond

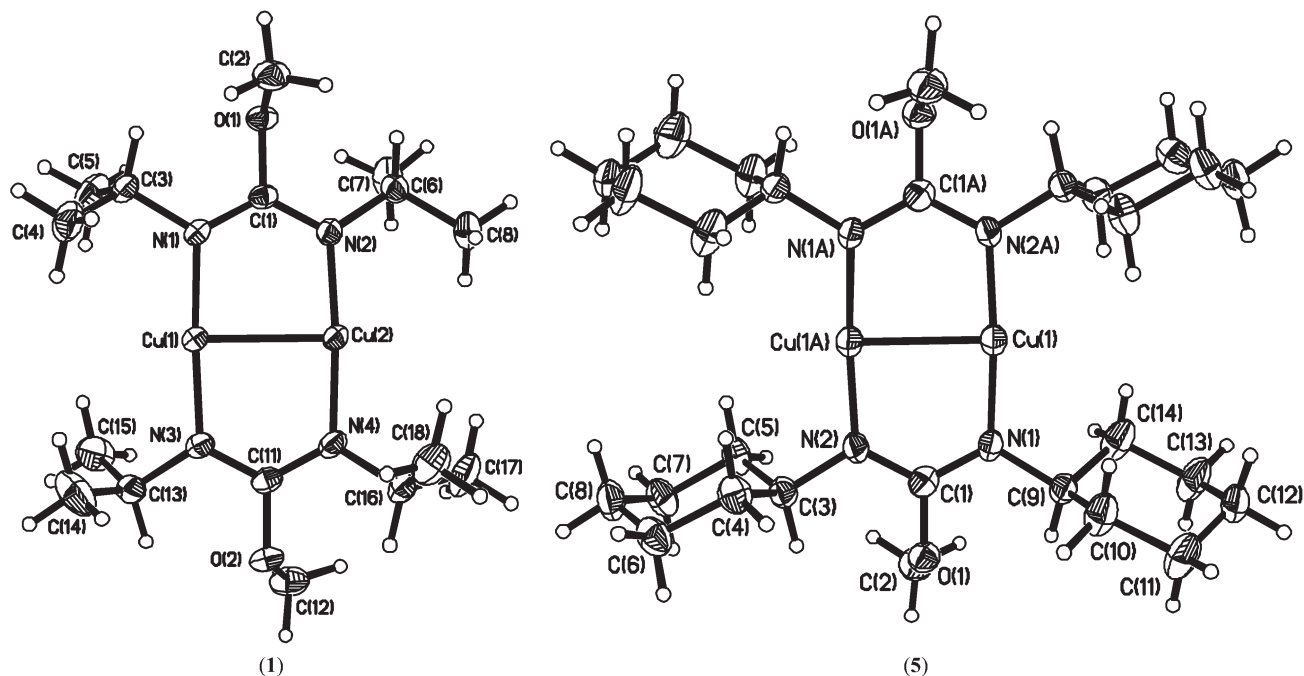


Fig. 2 Diagram showing the molecular structures of the complexes **1** and **5** (50% probability ellipsoids). Hydrogen atoms have been omitted for clarity. Symmetry transformations used to generate equivalent atoms in **5**: 2 - X, 1 - Y, -Z. Selected bond lengths (Å) and angles (°) for **1**: Cu(1)–Cu(2) 2.4653(4), Cu(1)–N(1) 1.877(2), Cu(1)–N(3) 1.872(2), Cu(2)–N(2) 1.879(2), C(1)–N(1) 1.321(3), C(1)–N(2) 1.324(3), C(11)–N(3) 1.325(3), C(11)–N(4) 1.322(3), C(1)–O(1) 1.384(3), C(11)–O(2) 1.382(3), O(1)–C(2) 1.447(3), O(2)–C(12) 1.447(3); N(1)–Cu(1)–N(3) 176.04(9), N(2)–Cu(2)–N(4) 175.11(9), N(1)–C(1)–N(2) 124.0(2), N(3)–C(11)–N(4) 123.8(2), C(1)–O(1)–C(2) 112.54(18), C(11)–O(2)–C(12) 112.23(19). Selected bond lengths (Å) and angles (°) for **5**: Cu(1)–Cu(1A) 2.4624(7), Cu(1)–N(1) 1.873(2), Cu(1)–N(2A) 1.874(2), C(1)–N(1) 1.321(4), C(1)–N(2) 1.321(4), C(1)–O(1) 1.380(3); N(1)–Cu(1)–N(2A) 175.83(10), N(1)–C(1)–N(2) 122.8(3), C(1)–O(1)–C(2) 112.9(2).

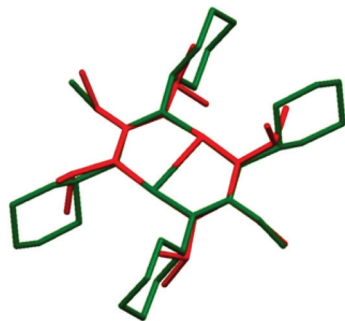


Fig. 3 Least-squares overlay of the two complexes **1** and **5** (**1** in red; **5** in green). RMS error of displacement over the two core $\{\text{Cu}_2(\text{N}_2\text{C})_2\}$ fragments is 1.24 Å.

length, of π -delocalisation into the $\{\text{NCN}\}$ core of the iso-ureate ligand. The bond angle belonging to the $\{\text{OR}\}$ substituents in complexes **1**–**5** are indicative of sp^2 hybridisation at the oxygen center. For delocalisation to occur within these iso-ureate ligands the $\{\text{Cu}_2(\text{N}_2\text{C})_2\}$ plane and that plane defined by the central C-atom of the iso-urea ligand and the $\{\text{OMe}\}$ group should be coplanar (Fig. 1); in **1** and **5** these planes are approaching a perpendicular arrangement [**1**: 72.17° , **5**: 86.29°]. This observation along with C–O bond lengths [**1**: 1.384(3) Å and 1.382(3) Å, **5**: 1.380(3) Å] suggest single bond character to the $\{\text{RO}-\text{CN}_2\}$ bond in the iso-ureate ligands. This observation is in contrast to guanidinate systems, where

C–NR₂ multiple bond character is typically ascribed. We must assume the apparent lack of C–O multiple bond character is a result of the increased electronegativity of oxygen compared to nitrogen in related guanidinate systems.

Thermal profile of complexes and use as deposition precursor

Thermogravimetric analysis (TGA) was performed on compounds **1**–**5** with all of the complexes leaving residues of between 23–31% of the original mass. Fig. 4 shows the TGA data for complex **1**–**5**. In the case complexes **1** and **2** the residual mass percentages observed (**1**: 25.8% and **2**: 24.4%) are all less than the expected residual mass % for the formation of pure copper (28.8% and 27.1% respectively), indicating that while some material has been lost due to sublimation, the majority of the product undergoes decomposition. Conversely, for complexes **3**–**5** the residual mass percentages observed (**3**: 26.0%, **4**: 28.13% and **5**: 24.2%) are higher than those expected for pure copper (25.6%, 24.2% and 21.1% respectively) suggesting carbon and/or oxygen incorporation into the residue. Of the complexes investigated compound **1** provided the sharpest decomposition profile. Once mass loss begins, it is relatively sharp for all but compound **5**, which has a temperature range of $>150^\circ\text{C}$, from the onset of mass loss ($\sim 195^\circ\text{C}$) to formation of a stable residue ($\sim 346^\circ\text{C}$). The $\{\text{O}^t\text{Bu}\}$ derivative **4**, shows a stepwise decomposition profile, with a slight plateau at 180°C corresponding to a mass loss of 40%, which is potentially due to the loss of one iso-urea ligand

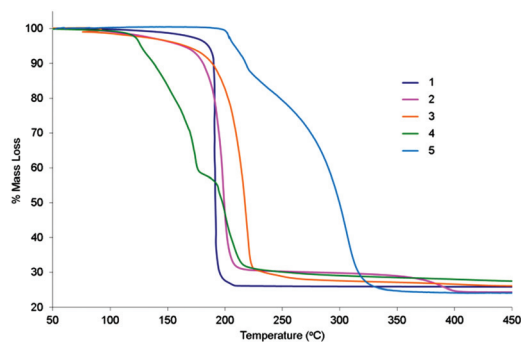


Fig. 4 The TGA data for complexes **1–5**. Experiments were run under N_2 (50 ml min^{-1}) at a ramp rate of $20 \text{ }^\circ\text{C min}^{-1}$.

during the first step in the TGA decomposition profile. Such observations are consistent with the proposed thermolysis mechanisms proposed by Barry and co-workers for related copper(i) guanidinate systems.^{14b}

All of the complexes, apart from **1**, decompose to give a stable residue that is a slightly higher value than that which corresponds to pure copper, indicating some contamination in the residue from ligand incorporation. Combined with a melting point of $96 \text{ }^\circ\text{C}$, lower than typical temperatures used for vapourisation, complex **1** was deemed a suitable candidate for assessment as a Cu deposition precursor.

Copper deposition and thin film analysis

Copper films were deposited using the iso-ureate complex **1** at low pressure in a hot-walled Electro-gas CVD apparatus. Films were deposited onto ruthenium coated silicon wafers, in an

Table 1 The general physical parameters for the low pressure CVD of complex **1**

Substrate temperature ($^\circ\text{C}$)	225	250	300
Operating pressure (Torr)	~ 30	~ 30	~ 30
Carrier gas	H_2	H_2	H_2
Carrier flow rate ($L \text{ min}^{-1}$)	0.3	0.3	0.3
Bubbler flow rate ($L \text{ min}^{-1}$)	0.3	0.3	0.3
Temp of precursor bubbler and carrier gas lines ($^\circ\text{C}$)	100	100	100
Deposition duration (min)	60	60	60

attempt to emulate industrially relevant substrates, where ruthenium is used as an adhesion layer for copper thin film deposition.³ The deposition of copper metal was investigated at three different substrate temperatures; $225 \text{ }^\circ\text{C}$, $250 \text{ }^\circ\text{C}$ and $300 \text{ }^\circ\text{C}$ respectively.

In all of the deposition runs the precursor and the carrier gas lines were externally heated to $100 \text{ }^\circ\text{C}$, and the pressure during deposition was maintained at 30 Torr. H_2 gas was used as the carrier gas at flow rates of 0.3 L min^{-1} . Table 1 shows the general physical parameters used throughout the deposition experiments.

Fig. 5 shows the top and cross-sectional SEM images of the thin film deposited at $225 \text{ }^\circ\text{C}$ (Fig. 5A and B) and $250 \text{ }^\circ\text{C}$ (Fig. 5D and E), respectively, alongside the AFM images (Fig. 5C: $225 \text{ }^\circ\text{C}$ and Fig. 5F: $250 \text{ }^\circ\text{C}$). Both films appear continuous and pin-hole free with submicron morphology consisting of particles, uniform in both size and shape (approx. $0.1 \mu\text{m}$ in dimension). Analysis of the AFM images show the films deposited at $250 \text{ }^\circ\text{C}$ to be marginally rougher ($225 \text{ }^\circ\text{C}$: $R_{\text{ms}} = 0.1107 \mu\text{m}$, $R_{\text{a}} = 0.0767 \mu\text{m}$, $250 \text{ }^\circ\text{C}$: $R_{\text{ms}} = 0.1278 \mu\text{m}$, $R_{\text{a}} = 0.0931 \mu\text{m}$). At both temperatures the deposited surfaces

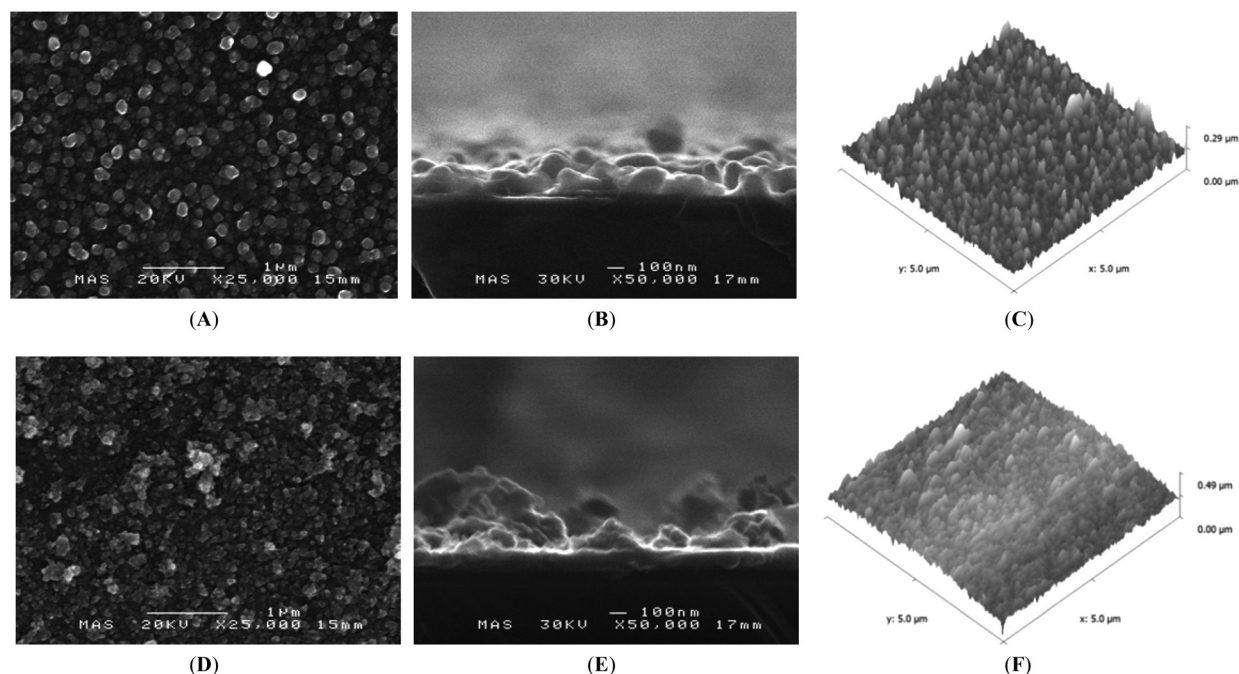


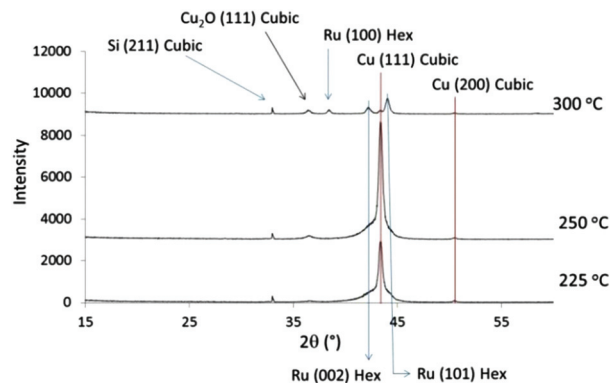
Fig. 5 SEM and AFM images of the thin films deposited from the copper precursor **1** at $225 \text{ }^\circ\text{C}$ (A–C) and $250 \text{ }^\circ\text{C}$ (D–F) respectively.

Table 2 PXRD peaks observed in films deposited on hexagonal Ru using **1** as precursor at 225 °C, 250 °C and 300 °C respectively

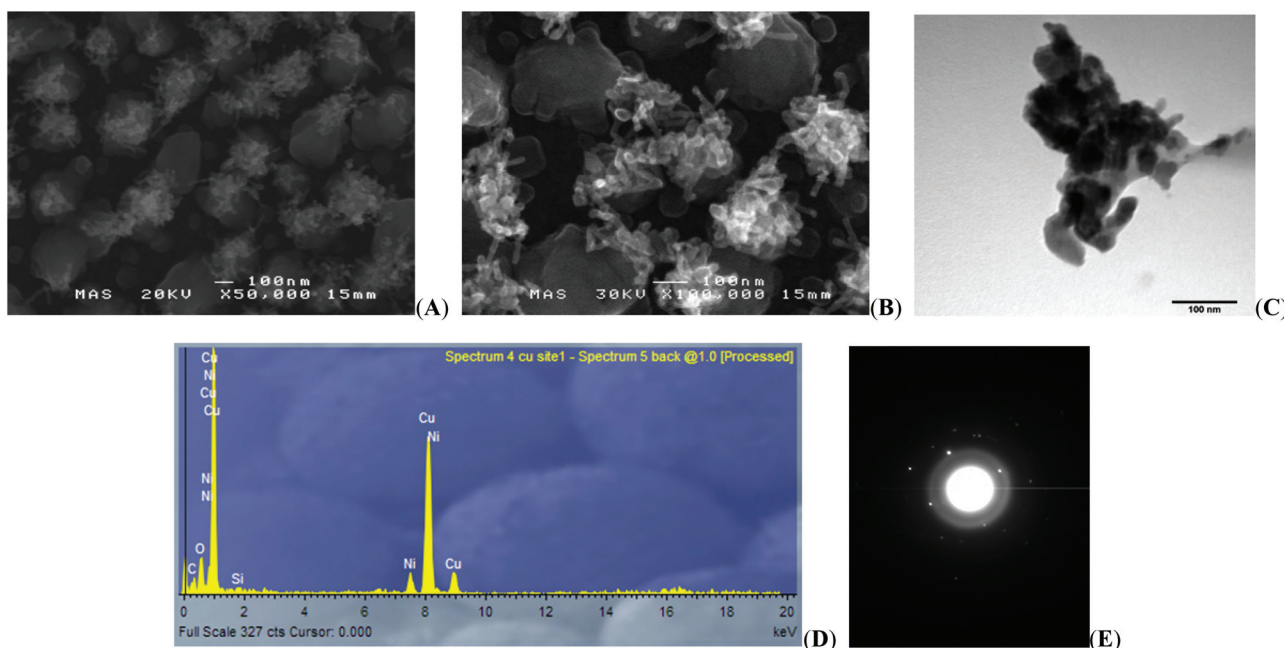
Element/compound	(hkl)	2θ	d (Å)	System	PDF number
Si	(211)	32.961	2.715	Cubic	72-1426
Cu ₂ O	(111)	36.403	2.466	Hex	78-2076
Ru	(100)	38.461	2.338	Hex	06-0663
Ru	(002)	42.222	2.138	Hex	06-0663
Ru	(101)	44.036	2.054	Hex	06-0663
Cu	(111)	43.339	2.083	Cubic	89-2838
Cu	(200)	50.508	1.805	Cubic	89-2838

are significantly rougher than desired for the microelectronics industry, although it is well documented that chemically deposited copper thin films are invariably irregular. It is also worth noting that the film roughness is in the same order of magnitude as film thickness (Fig. 5) and as such deposition run time will have a significant effect on roughness as would the possible future use of catalytic surfactants such as ethyl-iodide.²⁵ Because of the relative non-uniformity of the thickness across the sample, relative deposition rates could not be determined accurately.

Powder X-ray diffraction analysis of the films deposited onto ruthenium at 225 °C and 250 °C showed that they consist primarily of poly-crystalline copper metal, oriented in the (111) direction, together with some in the (200) direction (see Fig. 5 and Table 2). At a substrate deposition temperature of 300 °C the thin films produced were shown by SEM imaging to be significantly more uneven in appearance, with what appear to be nano-filaments emerging from the underlying crystalline copper (Fig. 7A and B). The uneven appearance of the films is

**Fig. 6** An overlay of the X-ray diffraction patterns derived from copper films deposited on hexagonal Ru using **1** as precursor at 225 °C, 250 °C and 300 °C respectively.

reinforced by the clear presence of substrate (*i.e.* Ru) in the PXRD pattern (Fig. 6) which is much harder to discern in the more continuous films grown at 225 °C and 250 °C respectively. Because of the much greater roughness of the surfaces of these films AFM images could not be obtained. In contrast films deposited onto ruthenium substrates at 300 °C appear from SEM images (Fig. 7) to be much more granular and uneven in their distribution with what appear to be 'flagella-like' nano-filament structures protruding from the larger particles (~0.2 μm), which are not observed in any of the films grown at lower temperatures. Samples of the copper filaments where examined independently of the underlying thin film, and shown by EDX to be pure copper (additional peaks of Ni/C/O in the EDX spectra come from the supporting grid).

**Fig. 7** SEM images of copper films grown on ruthenium substrate at 300 °C using complex **1** as a precursor (A and B). TEM images of copper filaments scratched off the underlying copper film (C). An EDX spectrum of the copper filaments (D). An electron diffraction pattern from the copper filaments showing them to be cubic copper metal (E).

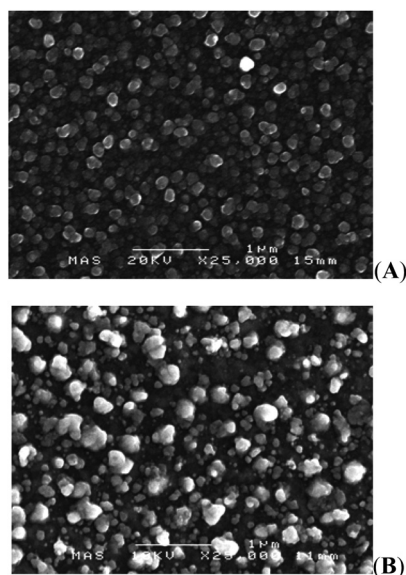


Fig. 8 SEM images of a copper film grown on ruthenium before (A) and after (B) thermal treatment (300 °C) under H₂ for 1 h.

Fig. 7e shows the electron diffraction pattern obtained from an examination of the filament structures, most likely to be looking along the (111) plane of the crystal (a distinction from the (002) plane could not be made), and highlights the highly crystalline nature of the filament structures.

It was therefore assumed that the nano-filament like structures, observed only on copper films deposited at 300 °C, are a result of either a thermally induced extrusion of copper from the underlying crystalline mass, or a result of thermally activated growth mechanism. In an attempt to test these hypotheses films grown at 225 °C, which appear as continuous films, were held at 300 °C under a flow of H₂ gas (0.6 L min⁻¹) at 50 Torr for 1 h. During this time, while copper filament growth was not observed, the rise in temperature of the substrate did induce significant surface mobility of the copper metal and subsequent growth of copper islands.

Successive deposition runs holding the substrate temperature at 300 °C using fresh precursor resulted in the formation of copper films with identical features.

SEM images of the film before and after thermal treatment (Fig. 8) show the formation of islands of copper and exposure of the underlying ruthenium substrates, an observation which is consistent with our PXRD results from direct film growth. Attempts to grow copper films on ruthenium substrates below 200 °C using complex **1** as a precursor proved to be challenging, primarily because of slow deposition rates.

It is therefore reasonable to assume that above 200 °C either the activation barrier to decomposition of **1** is overcome resulting in decomposition just above the wafer causing a copper seed layer to be deposited, or the thermal barrier to surface reaction is overcome.

EDX spectra of all the films (ESI[†]) show the presence of copper as well as small amounts of oxygen (less than 3% by EDX). PXRD analysis suggests that oxygen is present in the

Table 3 Atomic % elements in copper thin films deposited at 225 °C, 250 °C and 330 °C pre- and post-Ar etching (600 s)

	225 °C (pre)	225 °C (post)	250 °C (pre)	250 °C (post)	300 °C (pre)	300 °C (post)
Cu	54.11	96.88	11.31	81.78	4.96	80.12
C	37.16	—	62.58	8.58	65.89	10.96
O	8.73	0.37	26.11	9.64	29.87	8.93

form of Cu₂O. EDX spectroscopy also showed the presence of underlying substrate peaks (Fig. 6).

Atomic % analysis of the copper thin films was determined using XPS data at sputter etching times of 0 and 600 seconds for the films deposited at 225 °C, 250 °C and 300 °C respectively. Table 3 shows the relative atomic % contributions of Cu, C and O as determined by integration of the Cu 2p (931 eV), C 1s (284 eV) and O 1s (532 eV) binding energy peaks using the linear method both pre- and post-etched. XPS analysis of the untreated surface show peaks at binding energies of 284 eV and 532 eV which can be attributed to adsorbed carbon and oxygen containing organic species. After 600 s of Ar-etching these peaks are significantly reduced, as can be seen in Fig. 9, which shows the XPS spectra (both pre and post-etching) for the copper thin film deposited at 225 °C.

XPS analysis shows the atomic % of copper in films deposited at 225 °C (post-etching) to be 96.88 atomic %. XPS analysis also detects 2.75 atomic % of Ru metal, which is attributed to the underlying ruthenium substrate: if the underlying ruthenium is negated the atomic % of Cu and O rises to 99.62% and 0.38% respectively. The atomic % oxygen detected by XPS analysis in thin films deposited at 225 °C are within the levels associated with background levels for this very sensitive method of analysis.

The atomic % of oxygen recorded in the thin films deposited at 250 °C and 300 °C are higher than expected, suggestive of the possible incorporation of oxygen within the thin film from the thermal decomposition of ligands.

The observed high purity of these copper metal thin films is quite significant, as typical oxygen containing precursors are prone to the incorporation of oxygen into the deposited thin films.

The resistivity of films deposited at a substrate temperature of 225 °C measured using a 4-point probe was found to be 9.63 mΩ cm, approaching that of bulk copper (*cf.* 1.67 mΩ cm for bulk copper). Despite the high purity observed by XPS the higher than expected resistivity is likely to be a consequence of a number of factors, including film thinness, surface oxidation and relative unevenness of the film.

Conclusions

A new group of five copper(i) iso-ureate complexes have been synthesised and structurally characterised and shown to possess bimetallic structures in which the two iso-ureate ligands bridge a {Cu₂} core, such that each copper atom

Table 4 Crystal data and structure refinement for compounds 1–5

Compound	1	2	3	4	5
Chemical formula	C ₁₆ H ₃₄ Cu ₂ N ₄ O ₂	C ₁₈ H ₃₈ Cu ₂ N ₄ O ₂	C ₂₀ H ₄₂ Cu ₂ N ₄ O ₂	C ₂₂ H ₄₆ Cu ₂ N ₄ O ₂	C ₂₈ H ₅₀ Cu ₂ N ₄ O ₂
Formula mass	441.55	469.60	497.66	525.71	601.80
Crystal system	Triclinic	Monoclinic	Monoclinic	Orthorhombic	Monoclinic
<i>a</i> /Å	10.4470(2)	6.9630(2)	14.26300(10)	11.0610(2)	10.2090(4)
<i>b</i> /Å	11.9090(2)	16.1930(5)	10.37000(10)	12.9330(2)	11.2920(4)
<i>c</i> /Å	18.1380(3)	10.4080(3)	18.3100(2)	18.2690(2)	13.1660(6)
<i>α</i> /°	108.5190(10)	90.00	90.00	90.00	90.00
<i>β</i> /°	99.5910(10)	101.5790(10)	110.89	90.00	108.123(2)
<i>γ</i> /°	91.2370(10)	90.00	90.00	90.00	90.00
Unit cell volume/Å ³	2103.14(6)	1149.64(6)	2530.17(4)	2613.42(6)	1442.48(10)
Crystal size/mm ³	0.13 × 0.10 × 0.08	0.20 × 0.15 × 0.10	0.20 × 0.20 × 0.15	0.20 × 0.15 × 0.13	0.10 × 0.08 × 0.03
Temperature/K	150(2)	150(2)	150(2)	150(2)	150(2)
Space group	<i>P</i> 1	<i>P</i> 21/ <i>c</i>	<i>P</i> 21/ <i>c</i>	<i>Pcab</i>	<i>P</i> 21/ <i>c</i>
No. of formula units per unit cell, <i>Z</i>	4	2	4	4	2
Theta range for data collection	8.52 to 25.00°	3.21 to 27.56°	3.09 to 30.52°	3.65 to 28.28°	7.88 to 25.00°
Absorption coefficient, μ/mm ⁻¹	2.037	1.867	1.701	1.651	1.505
No. of reflections measured	21 281	21 623	52 560	40 255	10 591
No. of independent reflections	7077	2633	7717	3244	2449
Completeness	95.5%	99.3%	99.8%	99.8%	96.5%
<i>R</i> _{int}	0.0509	0.0499	0.0462	0.0528	0.0598
Final <i>R</i> ₁ values (<i>I</i> > 2σ(<i>I</i>))	0.0356	0.0320	0.0291	0.0266	0.0373
Final w <i>R</i> (<i>F</i> ²) values (<i>I</i> > 2σ(<i>I</i>))	0.0888	0.0727	0.0695	0.0635	0.0767
Final <i>R</i> ₁ values (all data)	0.0472	0.0448	0.0407	0.0380	0.0584
Final w <i>R</i> (<i>F</i> ²) values (all data)	0.0956	0.0788	0.0751	0.0687	0.0855
Goodness of fit on <i>F</i> ²	1.076	1.076	1.030	1.076	1.015
CCDC numbers	901461	901462	901463	901464	901465

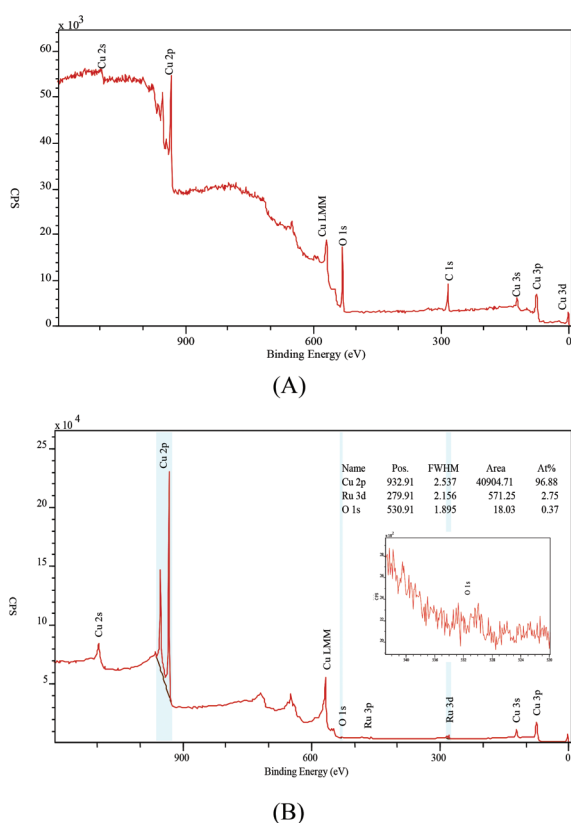


Fig. 9 XPS spectra of the copper thin films deposited using the precursor, 1, at 225 °C, pre-etching with Ar (A) and post etching with Ar (B).

possesses a linear two coordinate geometry. Amongst them the Cu(i) methoxy-*N,N'*-di-isopropyl-ureate (**1**) was found to be

especially attractive due its relatively low melting point, volatility and thermal reactivity.

Deposition was performed at three substrate temperatures (225 °C, 250 °C and 300 °C) under an atmosphere of hydrogen gas. Quite significantly, at all deposition temperatures, and especially at the lower deposition temperature of 225 °C investigated, crystalline pure copper metal was deposited, as evidenced by the analysis (PXRD, EDX and XPS). Removal of surface bound organic matter by Ar-etching reveals a high atomic percentage of copper metal (97–99 atomic %) at all deposition temperatures. At both 250 °C and 300 °C the atomic % of carbon is higher than expected, again suggesting possible carbon incorporation within the thin film from the thermal decomposition of the ligand systems. XPS spectra for films deposited at 250 °C and 300 °C are included in the ESI.†

Given the structural similarity between these new iso-ureate complexes and the structurally similar copper(i) amidinate and copper(i) guanidinate precursors described by Gordon *et al.*^{2a,c,e,f,h,j} and Barry *et al.*^{13,14} we may assume that comparable decomposition pathways are available to the precursors. At substrate temperatures below 200 °C deposition is arrested, presumably because thermal activation of the precursor above or at the surface is not achieved. At all deposition temperatures the growing copper thin films appears to prefer the cubic (111) orientation.

Copper films deposited at a substrate temperature of 300 °C were observed to be less regular/continuous than those deposited at 225 °C and 250 °C respectively: SEM images showing the presence of copper nano-filaments, which through experimentation were determined to be caused by high-temperature

growth mechanism, rather than an extrusion of the nano-filaments from the underlying copper films at elevated substrate temperatures.

Experimental

All manipulations were carried out under an atmosphere of dry dinitrogen or argon using standard Schlenk and glove-box techniques. Hexane, and THF were dried using an Innovative Technology, Inc. Solvent Purification System (SPS) system and degassed under dinitrogen or argon prior to use. The starting materials, di-isopropylcarbodiimide, di-cyclohexylcarbodiimide, CuCl, lithium bis(trimethylsilyl)amide, lithium hexamethyldisilylamide and potassium *tert*-butoxide were purchased from Aldrich Chemicals. Solution ^1H and ^{13}C NMR experiments were performed at ambient temperature using a Bruker Avance-300. ^1H and ^{13}C NMR chemical shifts are referenced internally to residual non-deuterated solvent resonances. All chemical shifts are reported in δ (ppm) and coupling constants in Hz. Elemental analyses were performed externally London Metropolitan University Microanalysis Service. Thermogravimetric analyses (TGA) were performed at SAFC Hitech using a Shimadzu TGA-51 Thermogravimetric Analyzer, while SEM-EDX analysis of the films was undertaken on a JEOL JSM-6480LV scanning electron microscope, FE-SEM analysis was undertaken on a JEOL 6301F microscope.

Synthesis of complex 1

Under an inert atmosphere (Ar), *N,N'*-diisopropylmethylisourea (0.91 ml, 5.00 mmol) in 20 ml of cold THF (-78°C) was added a Schlenk containing lithium bis(trimethylsilyl)amide (0.837 g, 5.00 mmol) and copper(I) chloride (0.495 g, 5.00 mmol). An immediate color change was observed, and the reaction was allowed to warm slowly to room temperature with constant stirring. After 1 hour the volatiles were removed under reduced pressure and dry hexane (20 ml) was added to the resultant residue. The hexane solution was left to stir for 15 minutes and the volatiles then removed under reduced pressure. This process was repeated on two further occasions to remove any residual THF. Further hexane (20 ml) was added and the slurry was filtered through Celite® to remove any insoluble materials. Concentration of the solution *in vacuo*, followed by storage at -28°C affords **1** as colorless crystals (0.81 g, 74%). Anal. Calc. for $\text{C}_{16}\text{H}_{34}\text{Cu}_2\text{N}_4\text{O}_2$: C, 43.62; H, 7.79; N, 12.73, found: C, 43.85; H, 7.53; N, 12.71%. M.p. = 95.6°C . ^1H NMR (CDCl_3 , 300.22 MHz) δ : 1.14 (d, 24H, $\text{NCH}(\text{CH}_3)_2$, $^3J = 6.32$ Hz), 3.68 (sept, 4H, $\text{NCH}(\text{CH}_3)_2$, $^3J = 6.32$ Hz), 3.70 (s, 6H, OCH_3). $^{13}\text{C}\{^1\text{H}\}$ NMR (CDCl_3 , 75.49 MHz) δ : 27.2 ($\text{NCH}(\text{CH}_3)_2$), 46.5 ($\text{NCH}(\text{CH}_3)_2$), 59.8 (OCH_3) 167.6 (NCN).

Synthesis of complex 2

Under an inert atmosphere (Ar), *N,N'*-diisopropylcarbodiimide (1.55 ml, 10.0 mmol) and copper(I) chloride (0.005 g, 0.05 mmol) were placed into a dry Schlenk tube. Anhydrous ethanol (6 ml, 103 mmol) was added by syringe and the

resulting clear pale green solution was allowed to stir for 18 hours, by which time the colour had changed to dark blue. Unreacted copper(I) chloride was removed by cannula filtration, and the filtrate combined with a solution of lithium bis(trimethylsilyl)amide (1.67 g, 10 mmol) in THF (10 ml). The reaction mixture was allowed to stir for 10 minutes. In the absence of light the solution was added to a slurry of copper(I) chloride (0.99 g, 10.0 mmol) in THF (10 ml) at -78°C and allowed to warm to room temperature. After stirring for 2 hours, the volatiles were removed under reduced pressure and dry hexane (20 ml) was added to the resultant residue. The hexane solution was left to stir for 15 minutes and the volatiles then removed under reduced pressure. This process was repeated on two further occasions to remove any residual THF and ethanol. Further hexane (20 ml) was added and the slurry was filtered through Celite® to remove any insoluble materials. Additional hexane (20 ml) was added, and the slurry was filtered through Celite® to remove any insoluble materials. Concentration of the solution *in vacuo*, followed by storage at -28°C affords **2** as pale yellow crystals (1.48 g, 63%). Anal. Calc. for $\text{C}_{18}\text{H}_{38}\text{Cu}_2\text{N}_4\text{O}_2$: C, 46.04, H, 8.16, N, 11.93, found: C, 45.43, H, 8.46, N, 11.5%. M.p. = 113.5°C . ^1H NMR (CDCl_3 , 300.22 MHz) δ : 1.14 (d, 24H, $\text{NCH}(\text{CH}_3)_2$, $^3J = 6.32$ Hz), 1.35 (t, 12H, OCH_2CH_3 , $^3J = 7.10$ Hz), 3.67 (sept, 4H, $\text{NCH}(\text{CH}_3)_2$, $^3J = 6.32$ Hz), 3.89 (q, 4H, OCH_2CH_3 , $^3J = 7.10$ Hz). $^{13}\text{C}\{^1\text{H}\}$ NMR (CDCl_3 , 75.49 MHz) δ : 15.2 (OCH_2CH_3), 27.3 ($\text{NCH}(\text{CH}_3)_2$), 46.6 ($\text{NCH}(\text{CH}_3)_2$), 67.9 (OCH_2CH_3), 166.9 (NCN).

Synthesis of complex 3

Complex **3** was synthesised in an analogous fashion to complex **2** using, isopropanol (0.89 ml, 11.6 mmol) to afford **3** as colorless crystals (1.74 g, 70%). Anal. Calc. for $\text{C}_{20}\text{H}_{42}\text{Cu}_2\text{N}_4\text{O}_2$: C, 48.27, H, 8.51, N, 11.26, found: C, 47.26, H, 8.18, N, 10.82%. M.p. = 119.2°C . ^1H NMR (CDCl_3 , 300.22 MHz) δ : 1.12 (d, 24H, $\text{NCH}(\text{CH}_3)_2$, $^3J = 6.48$ Hz), 1.13 (d, 12H, $\text{OCH}(\text{CH}_3)_2$, $^3J = 6.48$ Hz), 3.68 (sept, 4H, $\text{NCH}(\text{CH}_3)_2$, $^3J = 6.48$ Hz), 4.28 (sept, 2H, $\text{OCH}(\text{CH}_3)_2$, $^3J = 6.48$ Hz). $^{13}\text{C}\{^1\text{H}\}$ NMR (CDCl_3 , 75.49 MHz) δ : 22.6 ($\text{OCH}(\text{CH}_3)_2$), 27.4 ($\text{NCH}(\text{CH}_3)_2$), 47.2 ($\text{NCH}(\text{CH}_3)_2$), 73.8 ($\text{OCH}(\text{CH}_3)_2$), 165.3 (NCN).

Synthesis of complex 4

Under an inert atmosphere (Ar), potassium *tert*-butoxide (1.23 g, 11.0 mmol) was placed into a dry Schlenk followed by THF (10 ml). To this solution, *N,N'*-diisopropylcarbodiimide (1.55 ml, 10.0 mmol) was added *via* syringe and the reaction mixture left to stir for 2 hours. In the absence of light this solution was then added to a slurry of copper(I) chloride (0.99 g, 10.0 mmol) in THF and left to stir for 2 hours. The volatiles were removed under reduced pressure and dry hexane (20 ml) was added to the resultant residue. The hexane solution was left to stir for 15 minutes and the volatiles then removed under reduced pressure. This process was repeated on two further occasions to remove any residual THF. Further hexane (20 ml) was added and the slurry was filtered through Celite® to remove any insoluble materials. Concentration of

the solution *in vacuo*, followed by storage at $-28\text{ }^{\circ}\text{C}$ affords **4** as colorless crystals (1.81 g, 69%). Anal. Calc. for $\text{C}_{22}\text{H}_{46}\text{Cu}_2\text{N}_4\text{O}_2$: C, 50.26, H, 8.82, N, 10.66, found: C, 50.37, H, 8.74, N, 11.04%. M.p. = $121.3\text{ }^{\circ}\text{C}$. ^1H NMR (CDCl_3 , 300.22 MHz) δ : 1.11 (d, 24H, $\text{NCH}(\text{CH}_3)_2$, $^3J = 6.32\text{ Hz}$), 1.46 (s, 18H, $\text{OC}(\text{CH}_3)_3$), 3.80 (sept, 4H, $\text{NCH}(\text{CH}_3)_2$, $^3J = 6.32\text{ Hz}$). ^{13}C $\{^1\text{H}\}$ NMR (CDCl_3 , 75.49 MHz) δ : 28.0 ($\text{NCH}(\text{CH}_3)_2$), 30.0 ($\text{OC}(\text{CH}_3)_3$), 47.8 ($\text{NCH}(\text{CH}_3)_2$), 80.5 ($\text{OC}(\text{CH}_3)_3$), 165.7 (NCN).

Synthesis of complex 5

Complex **5** was synthesised in an analogous fashion to complex **2** using, methanol (8 ml, 200 mmol) and dicyclohexylcarbodiimide (2.06 g, 10.0 mmol), to afford **5** as colourless crystals (3.48 g, 58%). Anal. Calc. for $\text{C}_{28}\text{H}_{50}\text{Cu}_2\text{N}_4\text{O}_2$: C, 55.88, H, 8.37, N, 9.31, found: C, 56.19, H, 8.39, N, 9.03%. M.p. = dec. $137\text{ }^{\circ}\text{C}$, ^1H NMR (C_6D_6 , 300.22 MHz) δ : 1.21 (m, 8H, CH_2), 1.50 (m, 16H, $(\text{CH}_2)_2$), 1.64 (m, 16H, $(\text{CH}_2)_2$), 1.93, (m, 4, CH), 3.39 (s, 6H, $\text{O}(\text{CH}_3)$). $^{13}\text{C}\{^1\text{H}\}$ NMR (C_6D_6 , 75.49 MHz) δ : 26.7 (CH_2), 27.0 ($(\text{CH}_2)_2$), 39.7 ($(\text{CH}_2)_2$), 56.0 (N(CH)), 60.0 (OCH_3), 168.2 (NCN).

Materials chemistry

TGA analysis of the complexes was performed at SAFC Hitech, Bromborough, UK, using a Shimadzu TGA-51 Thermogravimetric Analyser. Data points were collected every second at a ramp rate of $20\text{ }^{\circ}\text{C min}^{-1}$ in a flowing (50 ml min^{-1}) N_2 stream. Thin films were deposited using a modified cold-walled CVD system (Electro-gas Systems Ltd, UK). The system consisted of a tubular quartz reactor containing a silicon carbide coated graphite susceptor. The temperature of the susceptor was monitored using a k-type thermocouple coupled with a proportional-integral-derivative controller (PID controller), and heated with a water cooled IR lamp mounted externally beneath the reaction tube. The pressure of the system was maintained at ~ 30 Torr throughout the deposition run, with the reactor lines and precursor, held in a bubbler, at $90\text{ }^{\circ}\text{C}$. The vapour generated was delivered to the reaction zone using a high purity Hydrogen (99.998%) carrier gas (300 ml min^{-1}) metered from a mass flow controller. Films were deposited onto CVD coated ruthenium on silicon wafers at a susceptor temperature of $300\text{ }^{\circ}\text{C}$. The total deposition time was 60 min.

X-ray photoelectron spectroscopy (XPS) measurements were performed on a Kratos Axis Ultra-DLD photoelectron spectrometer, utilising monochromatic Al $\text{K}\alpha$ radiation (photon energy 1486.6 eV), at the University of Cardiff. Spectra were calibrated to the Cu(2p) peak. Samples were sputtered for a pre-determined set time over a 4 mm square area using 4 kV argon ions from a minibeam I ion source. Spectra were collected at pass energies of 80 and 160 eV for high resolution and survey scans respectively, with the 100 μm aperture in place to focus on the center of the etch pit.

FE-SEM analysis of the films was undertaken on a JEOL 6301F. EDX analysis was performed using a JEOL 6480 LV SEM microscope. TEM analysis was undertaken on a JEOL 1200EX, using nickel grids, at the University of Bath.

AFM analysis was performed using a Digital Instruments Nanoscope IIIa, with TAP300 tips in contact mode (tip radius $< 10\text{ nm}$).

Powder XRD of the films was performed on a Bruker D8 Advance powder diffractometer, using a Cu anode X-ray source ($\text{K}\alpha$ wavelength = 1.5406 \AA) at the University of Bath.

Single crystal X-ray crystallography

Experimental details relating to the single-crystal X-ray crystallographic studies are summarised in Table 4. For all structures, data were collected on a Nonius Kappa CCD diffractometer at 150(2) K using Mo- $\text{K}\alpha$ radiation ($\lambda = 0.71073\text{ \AA}$). Structure solution and refinements were performed using SHELX86²⁶ and SHELX97²⁷ software, respectively. Corrections for absorption were made in all cases. Data were processed using the Nonius Software.²⁸ Structure solution,²⁹ followed by full-matrix least squares refinement^{27b} was performed using the WINGX-1.80 suite of programs throughout.³⁰ For all complexes, hydrogen atoms were included at calculated positions.

The molecular structure of complex **3** presents disorder in one of the isopropoxide (O^iPr) groups (atoms C27–C29 and C27A–C29A along with their associated hydrogen atoms) which was modeled anisotropically over two positions using an occupancy free variable.

Crystals of the complex **1** and **5** were both weakly diffracting, with substantial intensity loss at higher 2 theta angle. Hence a data completeness greater than 95.5% and 96.5% respectively (max $2\theta = 25.0^{\circ}$) could not be met. CCDC reference numbers 901461–901465.

Notes and references

- (a) J. R. Creighton and J. E. Parmeter, *Crit. Rev. Solid State Mater. Sci.*, 1993, **18**, 175–238; (b) M. J. Hampden-Smith and T. Kodas, *Polyhedron*, 1995, **14**, 699–732; (c) J. A. T. Norman, *J. Phys. IV*, 2001, **11**, Pr3-497–Pr3-503; (d) J. Rickerby and J. H. G. Steinke, *Chem. Rev.*, 2002, **102**, 1525–1549; (e) B. Luo and W. L. Gladfelter, *Chem. Vap. Deposition*, 2009, 320–356; (f) A. Grodzicki, I. Lakomska, P. Piszczek, I. Szymanska and E. Szlyk, *Coord. Chem. Rev.*, 2005, **249**, 2232–2258.
- (a) B. S. Lim, A. Rahtu and R. G. Gordon, *Nat. Mater.*, 2003, **2**, 749–754; (b) A. U. Mane and S. A. Shivashankar, *Mater. Sci. Semicond. Process.*, 2004, **7**, 343–347; (c) Z. Li, S. T. Barry and R. G. Gordon, *Inorg. Chem.*, 2005, **44**, 1728–1735; (d) K.-H. Park and W. J. Marshall, *J. Am. Chem. Soc.*, 2005, **127**, 9330–9331; (e) Z. Li and R. G. Gordon, *Chem. Vap. Deposition*, 2006, **12**, 435–441; (f) Z. Li, A. Rahtu and R. G. Gordon, *J. Electrochem. Soc.*, 2006, **153**, C787–C794; (g) K.-H. Park, Z. Bradley Alexander, S. Thompson Jeffery and J. Marshall Will, *Inorg. Chem.*, 2006, **45**, 8480–8482; (h) Q. Ma, H.-S. Guo, R. G. Gordon and F. Zaera, *Chem. Mater.*, 2010, **22**, 352–359; (i) B. Vidjayacoumar, D. J. H. Emslie, S. B. Clendenning, J. M. Blackwell,

- J. F. Britten and A. Rheingold, *Chem. Mater.*, 2010, **22**, 4844–4853; (j) Q. Ma, H. Guo, R. G. Gordon and F. Zaera, *Chem. Mater.*, 2011, **23**, 3325–3334; (k) G. Dey and S. D. Elliott, *J. Phys. Chem. A*, 2012, **116**, 8893–8901; (l) J. Huo, R. Solanki and J. McAndrew, *J. Mater. Res.*, 2002, **17**, 2394–2398.
- 3 (a) O. K. Kwon, J. H. Kim, H. S. Park and S. W. Kang, *J. Electrochem. Soc.*, 2004, **151**, G109–G112; (b) O. K. Kwon, S. H. Kwon, H. S. Park and S. W. Kang, *J. Electrochem. Soc.*, 2004, **151**, C753–C756.
- 4 (a) K. Ramasamy, M. A. Malik and P. O'Brien, *Chem. Sci.*, 2011, **2**, 1170–1172; (b) A. L. Abdelhady, M. A. Malik and P. O'Brien, *J. Mater. Chem.*, 2012, **22**, 3781–3785; (c) K. Ramasamy, M. A. Malik and P. O'Brien, *Chem. Commun.*, 2012, **48**, 5703–5714.
- 5 P. Jackson, D. Hariskos, E. Lotter, S. Paetel, R. Wuerz, R. Menner, W. Wischmann and M. Powalla, *Prog. Photovoltaics*, 2011, **19**, 894–897.
- 6 (a) C. Y. Cummings, G. Zoppi, I. Forbes, P. J. Dale, J. J. Scragg, L. M. Peter, G. Kociok-Kohn and F. Marken, *J. Electroanal. Chem.*, 2010, **645**, 16–21; (b) G. Zoppi, I. Forbes, R. W. Miles, P. J. Dale, J. J. Scragg and L. M. Peter, *Prog. Photovoltaics*, 2009, **17**, 315–319; (c) J. J. Scragg, P. J. Dale and L. M. Peter, *Thin Solid Films*, 2009, **517**, 2481–2484; (d) J. J. Scragg, P. J. Dale and L. M. Peter, *Electrochem. Commun.*, 2008, **10**, 639–642; (e) M. C. Artaud-Gillet, S. Duchemin, R. Odedra, G. Orsal, N. Rega, S. Rushworth and S. Siebentritt, *J. Cryst. Growth*, 2003, **252**, 626–627; (f) M. C. Artaud-Gillet, S. Duchemin, R. Odedra, G. Orsal, N. Rega, S. Rushworth and S. Siebentritt, *J. Cryst. Growth*, 2003, **248**, 163–168.
- 7 (a) D. W. Macomber and M. D. Rausch, *J. Am. Chem. Soc.*, 1983, **105**, 5325–5329; (b) D. B. Beach, W. F. Kane, F. K. Legoues and C. J. Knors, *Mater. Res. Soc. Symp. Proc.*, 1990, **181**, 73–77; (c) D. B. Beach, F. K. Legoues and C. K. Hu, *Chem. Mater.*, 1990, **2**, 216–219; (d) M. J. Hampdensmith, T. T. Kodas, M. Paffett, J. D. Farr and H. K. Shin, *Chem. Mater.*, 1990, **2**, 636–639.
- 8 (a) K. M. Chi, H. K. Shin, M. J. Hampdensmith, E. N. Duesler and T. T. Kodas, *Polyhedron*, 1991, **10**, 2293–2299; (b) K. M. Chi, H. K. Shin, M. J. Hampdensmith, T. T. Kodas and E. N. Duesler, *Inorg. Chem.*, 1991, **30**, 4293–4294; (c) H. K. Shin, K. M. Chi, M. J. Hampdensmith, T. T. Kodas, J. D. Farr and M. Paffett, *Adv. Mater.*, 1991, **3**, 246–248; (d) H. K. Shin, M. J. Hampdensmith, E. N. Duesler and T. T. Kodas, *Polyhedron*, 1991, **10**, 645–647; (e) T. H. Baum and C. E. Larson, *Chem. Mater.*, 1992, **4**, 365–369; (f) R. Kumar, F. R. Fronczek, A. W. Maverick, W. G. Lai and G. L. Griffin, *Chem. Mater.*, 1992, **4**, 577–582; (g) T. Kruck and C. Terfloth, *Chem. Ber.*, 1993, **126**, 1101–1106; (h) H. Y. Yoen, Y. B. Park and S. W. Rhee, *J. Mater. Sci.: Mater. Electron.*, 1997, **8**, 189–194; (i) J. H. Son, M. Y. Park and S. W. Rhee, *Thin Solid Films*, 1998, **335**, 229–236; (j) S. W. Kang, S. H. Han and S. W. Rhee, *Thin Solid Films*, 1999, **350**, 10–13; (k) M. Y. Park, J. H. Son, S. W. Kang and S. W. Rhee, *J. Mater. Res.*, 1999, **14**, 975–979; (l) B. A. Kim and H. H. Lee, *Chem. Vap. Deposition*, 2001, **7**, 242–245.
- 9 (a) H. K. Shin, M. J. Hampdensmith, T. T. Kodas and A. L. Rheingold, *J. Chem. Soc., Chem. Commun.*, 1992, 217–219; (b) M. Becht, T. Gerfin and K. H. Dahmen, *Helv. Chim. Acta*, 1994, **77**, 1288–1298.
- 10 H. Guillon, S. Daniele, L. G. Hubert-Pfalzgraf and C. Bavoux, *Inorg. Chim. Acta*, 2000, **304**, 99–107.
- 11 (a) A. Jakob, T. Ruffer, P. Ecorchard, B. Walfort, K. Korbitz, S. Fruhauf, S. E. Schulz, T. Gessner and H. Lang, *Z. Anorg. Allg. Chem.*, 2010, **636**, 1931–1940; (b) R. Mothes, T. Ruffer, Y. Z. Shen, A. Jakob, B. Walfort, H. Petzold, S. E. Schulz, R. Ecke, T. Gessner and H. Lang, *Dalton Trans.*, 2010, **39**, 11235–11247; (c) W. B. Szymanska, P. Piszczek and E. Szlyk, *Polyhedron*, 2009, **28**, 721–728; (d) J. L. Han, Y. Z. Shen, C. X. Li, Y. Z. Li and Y. Pan, *Inorg. Chim. Acta*, 2005, **358**, 4417–4422; (e) A. Jakob, H. Schmidt, B. Walfort, G. Rheinwald, S. Fruhauf, S. Schulz, T. Gessner and H. Lang, *Z. Anorg. Allg. Chem.*, 2005, **631**, 1079–1086.
- 12 (a) Y. Chi, P. F. Hsu, C. S. Liu, W. L. Ching, T. Y. Chou, A. J. Carty, S. M. Peng, G. H. Lee and S. H. Chuang, *J. Mater. Chem.*, 2002, **12**, 3541–3550; (b) M. Veith, N. Lecerf, S. Mathur, H. Shen and S. Hufner, *Chem. Mater.*, 1999, **11**, 3103–3112.
- 13 T. J. J. Whitehorne, J. P. Coyle, A. Mahmood, W. H. Monillas, G. P. A. Yap and S. T. Barry, *Eur. J. Inorg. Chem.*, 2011, 3240–3247.
- 14 (a) J. P. Coyle, W. H. Monillas, G. P. A. Yap and S. T. Barry, *Inorg. Chem.*, 2008, **47**, 683–689; (b) J. P. Coyle, P. A. Johnson, G. A. DiLabio, S. T. Barry and J. Muller, *Inorg. Chem.*, 2010, **49**, 2844–2850; (c) A. M. Willcocks, T. P. Robinson, C. Roche, T. Pugh, S. P. Richards, A. J. Kingsley, J. P. Lowe and A. L. Johnson, *Inorg. Chem.*, 2012, **51**, 246–257.
- 15 L. J. Mathias, *Org. Prep. Proced. Int.*, 1980, **12**, 309–326.
- 16 N. Matsumura, T. Ohba and H. Inoue, *Bull. Chem. Soc. Jpn.*, 1982, **55**, 3949–3950.
- 17 H.-Z. Tang, D. Boyle Paul and M. Novak Bruce, *J. Am. Chem. Soc.*, 2005, **127**, 2136–2142.
- 18 (a) A. J. Bloodworth, A. G. Davies and S. C. Vasishtha, *J. Chem. Soc. C*, 1967, 1309–1313; (b) A. G. Davies, (M and T Chemicals Inc.), *Application: US* 1964-406571, 1967; (c) I. Shibata, H. Yamasaki, A. Baba and H. Matsuda, *J. Org. Chem.*, 1992, **57**, 6909–6914.
- 19 (a) A. G. Davies and R. J. Puddephatt, *J. Organomet. Chem.*, 1966, **5**, 590–592; (b) A. G. Davies and R. J. Puddephatt, *J. Chem. Soc. C*, 1967, 2663–2668.
- 20 (a) T. A. Budzichowski, M. H. Chisholm, K. Folting, J. C. Huffman, W. E. Streib and D. B. Tiedtke, *Polyhedron*, 1998, **17**, 857–867; (b) Y. Cao, Z. Du, W. B. Li, J. M. Li, Y. Zhang, F. Xu and Q. Shen, *Inorg. Chem.*, 2011, **50**, 3729–3737; (c) Z. Du, Y. Zhang, Y. M. Yao and Q. Shen, *Dalton Trans.*, 2011, **40**, 7639–7644; (d) Z. Du, H. Zhou, H. S. Yao, Y. Zhang, Y. M. Yao and Q. Shen, *Chem. Commun.*, 2011, **47**, 3595–3597.

- 21 (a) M. Bortoluzzi, G. Paolucci, F. Sartor and V. Bertolasi, *Polyhedron*, 2012, **37**, 66–76; (b) B. M. Bycroft and J. D. Cotton, *J. Chem. Soc., Dalton Trans.*, 1973, 1867–1870; (c) J. Vicente, J. A. Abad, M.-J. Lopez-Saez and P. G. Jones, *Organometallics*, 2006, **25**, 1851–1853; (d) J. Vicente, J.-A. Abad, M.-J. Lopez-Saez, P. G. Jones and D. Bautista, *Chem.–Eur. J.*, 2010, **16**, 661–676; (e) F. W. B. Einstein and J. S. Field, *Acta Crystallogr., Sect. B: Struct. Crystallogr. Cryst. Chem.*, 1979, **35**, 1696–1698; (f) Y. J. Park, N. S. Sickerman, J. W. Ziller and A. S. Borovik, *Chem. Commun.*, 2010, **46**, 2584–2586.
- 22 (a) I. Westmoreland, I. J. Munslow, A. J. Clarke, G. Clarkson and P. Scott, *Organometallics*, 2004, **23**, 5066–5074; (b) A. L. Gott, S. R. Coles, A. J. Clarke, G. J. Clarkson and P. Scott, *Organometallics*, 2007, **26**, 136–142.
- 23 T. Chen, C. Xu, T. H. Baum, B. C. Hendrix, T. Cameron, J. F. Roeder and M. Stender, (Advanced Technology Materials, Inc., USA), *Application: WO 2007142700*, 2007.
- 24 A. L. Johnson, A. M. Willcocks and S. P. Richards, *Inorg. Chem.*, 2009, **48**, 8613–8622.
- 25 E. S. Hwang and J. Lee, *Chem. Mater.*, 2000, **12**, 2076–2081.
- 26 G. M. Sheldrick, *SHELX-86, Computer Program for Crystal Structure Determination*, University Of Göttingen, Germany, 1986.
- 27 (a) G. M. Sheldrick, *SHELX-97, Computer Program for Crystal Structure Refinement*, University of Göttingen, Germany, 1997; (b) G. M. Sheldrick, *Acta Crystallogr., Sect. A: Fundam. Crystallogr.*, 2008, **64**, 112–122.
- 28 Z. Otwinowski and W. Minor, *Methods Enzymol.*, 1997, **276**, 307–326.
- 29 A. Altomare, M. C. Burla, M. Camalli, G. L. Cascarano, C. Giacovazzo, A. Guagliardi, A. G. G. Moliterni, G. Polidori and R. Spagna, *J. Appl. Crystallogr.*, 1999, **32**, 115–119.
- 30 L. J. Farrugia, *J. Appl. Crystallogr.*, 2012, **45**, 849–854.